JOURNAL OF SPACECRAFT AND ROCKETS
Vol. 34, No. 5, September–October 1997

High-Fidelity Thermal Protection System Sizing of Reusable Launch Vehicle

G. E. Palmer,* W. D. Henline,* D. R. Olynick,* and F. S. Milos†
NASA Ames Research Center, Moffett Field, California 94035

A coupled computational fluid dynamics/in-depth conduction analysis procedure to perform high-fidelity thermal protection system sizing is presented. The thermal environment on the vehicle surface, including radiative equilibrium wall temperature and surface catalycity, is computed using a real-gas, Navier–Stokes flow solver. Based on the computed surface temperatures, a thermal protection system material mapping is performed. Material thickness and overall thermal protection system mass are obtained using an in-depth conduction code. This procedure is used to size the thermal protection system on a lifting-body, single-stage-to-orbit vehicle.

Nomenclature

h_s = enthalpy of species s
k = Boltzmann constant, 1.3805×10^{-23} J/K
m_s = molar mass of species s
q_{cond} = conductive heat flux
T_w = wall temperature
u_s = velocity of species s normal to wall
ε = surface emissivity
η = surface normal direction
κ = thermal conductivity
ρ_s = density of species s
σ = Stefan–Boltzmann constant

Introduction

IN 1993, NASA began a study to define and analyze the launch requirements for the first part of the 21st century. This study became known as the Access to Space program.[1] The primary goal of this study was to identify systems that would improve safety and reduce operations cost. One option identified by the study was to improve the Shuttle fleet to allow continued operations through 2030. A second option was to replace the Shuttle with a fleet of expendable launch vehicles by 2005.

A third option was to replace the Shuttle fleet by the year 2008 with a fleet of fully reusable single-stage-to-orbit (SSTO) launch vehicles that would use advanced technologies to meet the requirements of improved safety and reduced operations cost. The vehicles must accommodate Space Station resupply and 20,000- to 25,000-lb mass satellite deployment missions.

Three potential reusable SSTO vehicle configurations were under consideration. The first was a vertical-takeoff/horizontal-landing wing-body concept. The second concept was a vertical-takeoff/vertical-landing vehicle. The third vehicle evaluated under the Access to Space reusable SSTO study was a vertical-takeoff/horizontal-landing lifting body.[2] The vehicle shape is similar to the lifting bodies tested during the 1960s.

To maximize payload for any SSTO vehicle, it is critical to minimize the structural weight of the vehicle. The purpose of this study is to present a methodology that will produce a high-fidelity sizing of the vehicle thermal protection system (TPS). This methodology is applied to assess the thermal environment on the surface of a lifting-body SSTO vehicle during its descent trajectory and to size the vehicle's TPS. The six-step analysis process is as follows.

1) Generate three-dimensional volume grids over the vehicle geometry with adequate spatial resolution to accurately compute surface heating and temperature.

2) Obtain the approximate location of peak heating by solving the three-dimensional Navier–Stokes equations at selected points along the vehicle's descent trajectory using a constant-temperature, noncatalytic wall boundary condition at the vehicle surface.

3) Perform a fully catalytic, radiative equilibrium wall flow solution at the peak heating point to obtain a conservative estimate of temperatures on the vehicle surface.

4) Create a TPS material mapping on the vehicle surface using the surface temperatures from the fully catalytic peak heating solution and the maximum reuse temperatures of the candidate TPS materials. The Access to Space baseline TPS materials were used: advanced carbon–carbon (ACC),[3] tailorable advanced blanket insulation (TABI),[4] and advanced flexible reusable surface insulation (AFRSI).[5]

5) Compute finite rate catalytic flow solutions at selected points along the vehicle's descent trajectory using material and temperature wall functions at each body point corresponding to the TPS material mapping at that point. This yields the convective heating and recovery temperature at each point on the vehicle surface.

6) Use the one-dimensional, in-depth conduction code OMLITS to compute required TPS thickness subject to bond-line and material temperature limits. The overall weight of the TPS then can be estimated.

Analysis Tools

Grid Generation

Figure 1 shows the lifting-body vehicle geometry. The overall vehicle length is just over 105 ft and consists of a delta planform with a blunted nose. The lower forebody surface is spherical with a large radius of curvature. A cylindrical payload bay is situated on the vehicle centerline. On either side of the payload bay are conical liquid hydrogen tanks. A liquid oxygen tank is located aft of the payload bay. The lifting body has two canted vertical tails for aerodynamic stability and control.

The elliptic grid generator GRIDGEN[6] was used to generate three-dimensional volume grids over the vehicle surface. GRIDGEN distributes points in the three-dimensional domain bounded by the body surface and outer grid planes by solving a series of partial differential equations. Outer boundary definition and point distribution as well as initial grid spacing and distribution function at the body surface are user specified. The grid used for the gasdynamic calculations consisted of 60 streamwise, 58 circumferential, and 79 body-normal grid points. The first grid spacing normal to the body was set to $1.0e{-}6$ m.

Presented as Paper 95-2080 at the AIAA 29th Thermophysics Conference, San Diego, CA, June 19–22, 1995; received Aug. 23, 1996; revision received April 15, 1997; accepted for publication June 28, 1997.

*Research Scientist, Reacting Flow Environments Branch. Senior Member AIAA.

†Aerospace Engineer, Thermal Protection Materials and Systems Branch. Member AIAA.

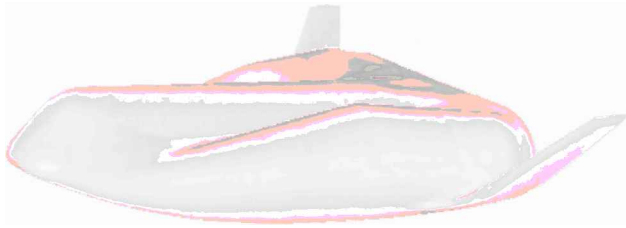

Fig. 1 Lifting-body surface geometry.

Gasdynamic Solution Algorithm

Flow solutions over the lifting body were performed using the GASP flow solver.[7] GASP is a general-purpose finite volume code that solves the time-dependent, three-dimensional, Navier–Stokes equations. Built into GASP are a number of chemical, turbulence, and thermodynamic models. For the solutions described in this study, a seven-species, one-temperature air chemistry model was used. Thermodynamic properties are evaluated using the Lewis curve fits for specific heat.[8] Blottner curve fits are used to evaluate species laminar viscosity.[9] Thermal conductivity is obtained using Eucken's relation.[7] Diffusion is modeled using a binary diffusion model with constant Schmidt number.

Inviscid flux terms are evaluated using third-order, upwind-biased, Van Leer flux vector splitting.[10] MUSCL interpolation with the minmod limiter[11] is used to achieve the higher-order spatial accuracy. The implicit solution algorithm used is two-factor approximate factorization with sweeping in the streamwise direction.

For use in this and other Access to Space design studies,[12,13] sophisticated surface boundary conditions were built into the GASP flow solver. Previously, GASP used a constant-temperature, noncatalytic wall boundary condition. A more realistic boundary condition is to compute the wall temperature by evaluating an energy balance at the body surface[12]:

$$\kappa \frac{\partial T}{\partial \eta} - \sum \rho_s u_s h_s = \sigma \varepsilon T_w^4 + q_{\text{cond}} \tag{1}$$

The terms on the left-hand side of Eq. (1) represent energy transmitted from the fluid to the wall via convection and diffusion. The terms on the right-hand side of Eq. (1) are the energy transferred from the wall to the fluid due to radiation and into the TPS layer and vehicle structure due to conduction.

The TPS materials are catalytic, in that atomic oxygen and nitrogen recombine at the material surface. Because of mass conservation, the species diffusion rate at the wall is equal to the net rate of disappearance of the species by surface reactions. The net rate of disappearance is modeled using first-order reaction rates, and the mass balance becomes[12]

$$-\rho_s u_s = \rho_s \gamma_s \sqrt{\frac{kT_w}{2\pi m_s}} \tag{2}$$

The quantity γ_s is the species recombination coefficient and is a function of temperature.[14]

In-Depth Conduction Code

Once the TPS material mapping has been obtained, and the radiative equilibrium, finite rate catalytic temperatures, and heat loads at the vehicle surface have been computed, the TPS material thickness must be determined at each body point so that maximum material and structural temperature limits are not exceeded. To obtain this information, it is necessary to solve the transient in-depth conduction into the TPS/structure material stackup. This analysis must not only compute the temperature profile due to the surface heat flux at a given time but also must account for the accumulation of thermal energy due to the heat flux at all previous times in the vehicle's trajectory.

The one-dimensional, in-depth conduction code OMLITS[15] is used. Details on the in-depth conduction governing equations and solution methodology can be found in Ref. 13. A rigorous solution methodolgy would solve the gasdynamic and in-depth conduction governing equations simultaneously. This is impractical for a three-dimensional vehicle such as the lifting body because of the computational expense this would entail. Instead, the conduction code was used as a postprocessor. The surface heat fluxes and temperatures at selected points along the vehicle trajectory obtained from the gasdynamic solver served as anchor points for the conduction code, which computed the temperature profile throughout the TPS/structural material layer at each body point along the entire trajectory.

Results

Gasdynamic Code Validation

Results from the GASP flow solver have been previously compared against experimental and flight data.[16,17] In Ref. 16, computational results for flow over the Space Shuttle Orbiter using finite rate, radiative equilibrium wall boundary conditions were compared against flight data taken during the STS-2 flight. One of the comparisons preformed was at the flight conditions corresponding to an altitude of 72.4 km during the vehicle's descent trajectory. In the present work, a flow solution is generated at the 72.4-km trajectory point using GASP with a five-species, one-temperature chemistry model and a radiative equilibrium wall boundary condition with reaction-cured glass surface kinetics[18] and a constant emissivity of 0.85. Laminar flow was assumed. The grid used in the calculation employed 80 points axially, 75 points tangentially, and 51 points normal to the surface. The comparison between the GASP solution and the STS-2 flight data is shown in Fig. 2.

In Ref. 17, numerical surface heating results were compared against fight data at 11 locations on the surface of the Space Shuttle during the STS-2 flight. A total of 22 three-dimensional computational fluid dynamics (CFD) computations were performed at 8 points along the descent trajectory using various grid-point densities, surface kinetics, and chemistry models. For most of the cases investigated, the CFD data compared closely with the flight data on the windward surfaces.

Although these two references do not represent a comprehensive validation of the gasdynamic solver, the ability of the code to reproduce flight heating data over the windward surface of the Space Shuttle along a substantial portion of the STS-2 descent trajectory demonstrates the applicability of the code to the high-fidelity TPS sizing methodology.

Noncatalytic Gasdynamic Results

The first step in the high-fidelity TPS sizing is to find the approximate point of peak heating. The descent trajectory curve is shown in Fig. 3. Computations were performed at the 80-, 75-, 70-, 60-, and 50-km points using a noncatalytic wall boundary condition with a constant wall temperature of 1500 K. This first series of computations could be performed using a fully catalytic wall boundary condition, but this boundary condition is not as stable as the

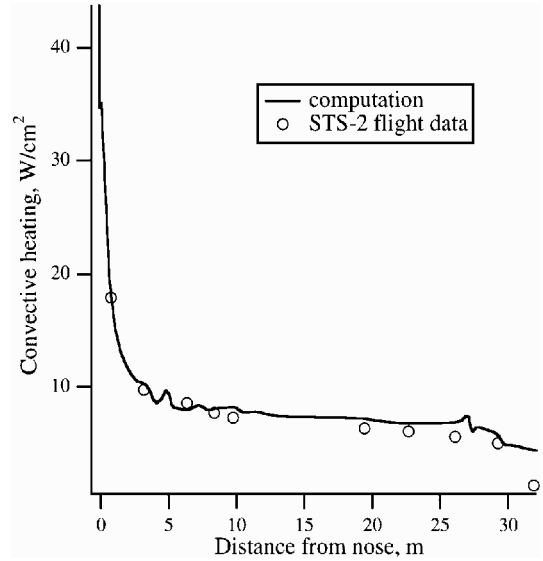

Fig. 2 Heating profiles along Shuttle windward centerline.

noncatalytic boundary condition. A seven-species, one-temperature air chemistry model was used for all five computations. Laminar flow was assumed. At the higher altitudes, 75 and 80 km, the gas behind the shock wave would be in thermochemical nonequilibrium. Because the purpose of these calculations was to determine the heat transfer to the body surface and because temperatures would tend to equilibrate near the body surface, a one-temperature model was deemed satisfactory for all five computations.

The windward and leeward centerline heating profiles plotted as a function of distance from the vehicle nose are shown in Fig. 4. On these and subsequent plots, a positive distance indicates the windward side of the vehicle and a negative distance the leeward. The heating profiles are essentially the same for the 60-, 70-, and 75-km trajectory points. The increased freestream density encountered as the vehicle descends from 75 to 60 km is balanced by decreasing velocity, resulting in a fairly constant centerline heating profile with a stagnation-point value approximately 40% higher than that experienced at 80 km. The 75-km case showed a slightly higher stagnation-point heating, and this trajectory point was used for the subsequent fully catalytic computation. At 50 km, the freestream Mach number had dropped to 7.85 and the windward centerline heating was about half that seen at the 60- to 75-km trajectory points. The leeward-side heating profile was nearly identical for the 60-, 70-, 75-, and 80-km calculations, dropping off sharply as the flow expanded around the vehicle nose.

The minmod limiter was used in all calculations to achieve higher-order spatial accuracy. The residual drops slightly more than three orders of magnitude before leveling off in an oscillatory fashion, as shown in Fig. 5a. This leveling off/oscillatory behavior is characteristic of the minmod limiter. Another way to evaluate solution convergence is to examine the evolution of the centerline heating profile, shown in Fig. 5b. As the solution progresses, the heating profile asymptotically approaches a steady-state curve.

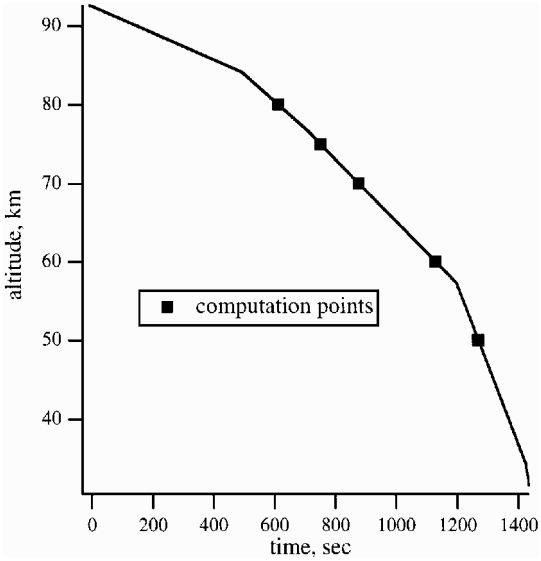

Fig. 3 Lifting-body trajectory.

TPS Material Mapping

To determine the maximum temperature at the vehicle surface, a fully catalytic, radiative equilibrium wall solution was run at the 75-km trajectory point. In reality, the TPS materials are not fully catalytic. Assuming a fully catalytic surface, where the recombination coefficients for all species are one, yields higher surface temperatures than if a finite rate catalytic surface model, where the recombination coefficients are between zero and one, is used. Therefore the fully catalytic solution should yield a conservative estimate of surface temperatures. The leeward and windward centerline temperature profiles are shown in Fig. 6. The maximum reuse temperatures for ACC, TABI, and AFRSI (1866, 1366, and 922 K, respectively) also are shown.

On the basis of fully catalytic surface temperatures, a TPS material was assigned to each surface area on the vehicle. The resulting material map is shown in Fig. 7. The areas covered with ACC are shown in black. ACC is required only around the stagnation point near the vehicle nose and on the wing leading edge, where the maximum heating rates and surface temperatures occur. The area covered by TABI is shown in gray. TABI covers most of the windward side of the vehicle as well as part of the leeward side of the wing and near the nose. The area covered with AFRSI is shown in light gray. AFRSI can be used over most of the leeward side of the vehicle.

A layer of Rhoacell® foam is used as TPS backup insulation between the surface material (TABI or AFRSI) and the liquid oxygen (LOX) and liquid hydrogen (LH_2) tanks. The Rhoacell prevents the room-temperature vulcanization (RTV) bondline used to secure the TPS material from dropping below 166 K. Below this temperature, the RTV becomes brittle. The LH_2 tanks are covered with a 25.4-mm layer of foam, and the LOX tank is protected with 20.32 mm of foam.

Finite Rate Catalytic Gasdynamic Solutions

Using the TPS material map, gasdynamic solutions were recomputed at the five trajectory points using the finite rate catalytic, radiative equilibrium wall boundary condition. The centerline convective heating profiles are displayed in Fig. 8. The profiles are

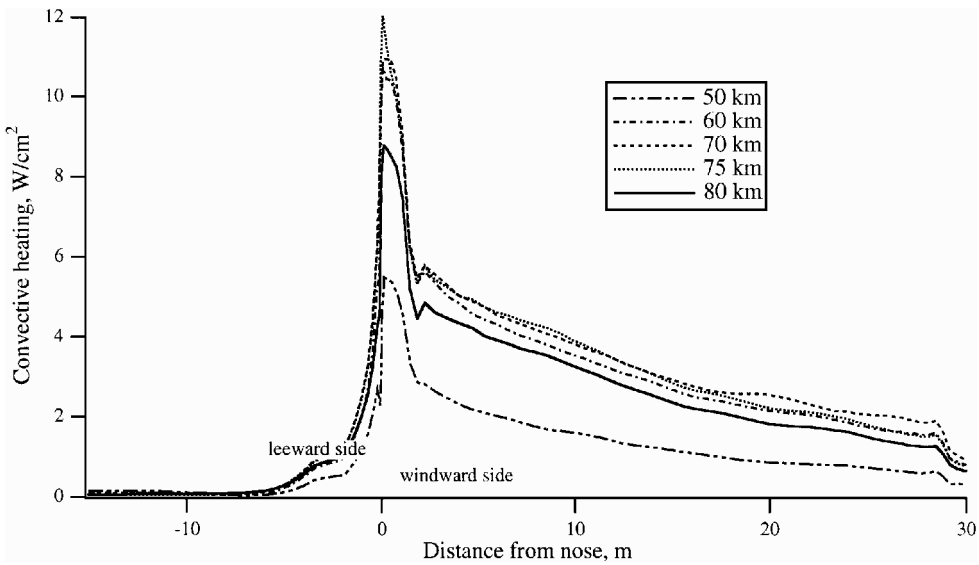

Fig. 4 Constant-temperature, noncatalytic heating profile.

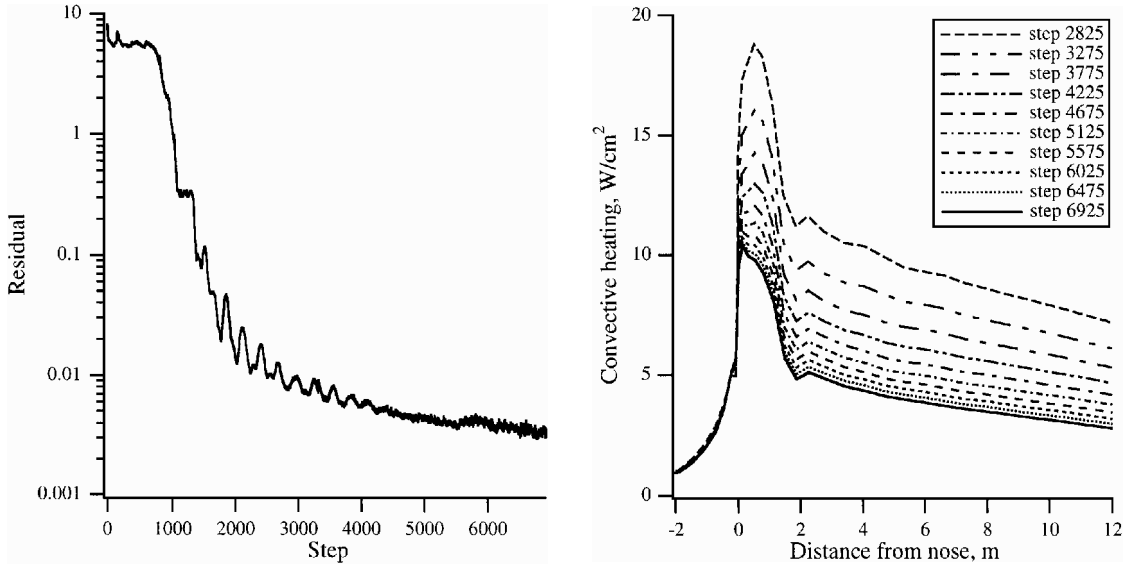

a) Residual b) Centerline heating

Fig. 5 Convergence histories, 60-km computation.

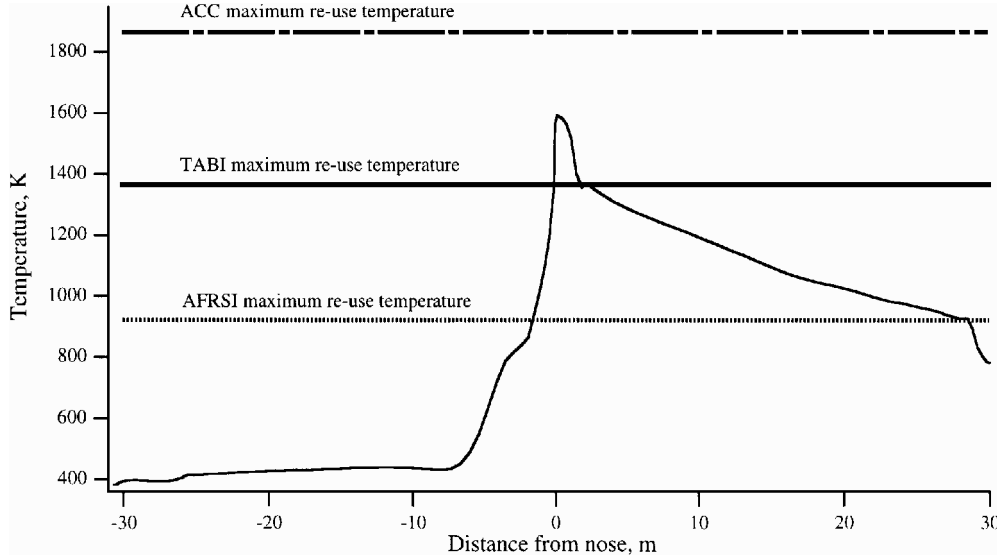

Fig. 6 Centerline temperature profile, 75-km, fully catalytic solution.

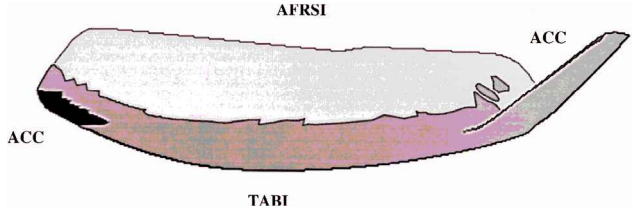

Fig. 7 TPS material mapping.

similar to the constant-temperature, noncatalytic curves except that the heating values are higher. There is a spike in the heating profile at $x = 4.04$ m on the windward side, corresponding to the ACC–TABI interface. This spike is due to the difference in surface catalycity between the two materials. A detailed description of this phenomenon is provided in Ref. 12. The spike in the heating profile at 2.7 m is seen in all of the computational profiles and is due to an anomaly in the surface grid.

The peak heating point in the finite rate catalytic solutions occurs somewhere between 70- and 75-km altitude. The laminar flow assumption is reasonable at these altitudes. The vehicle would experience turbulent flow at lower altitudes. Turbulent surface heating rates can be significantly higher than laminar surface heating rates. The point along the trajectory where the flow becomes turbulent cannot be determined analytically and must be obtained experimentally. Because the main focus of this paper is to present the high-fidelity TPS sizing methodology and no experimental transition data exist, the laminar flow assumption was used at all trajectory points studied.

Figure 9 shows fully catalytic and finite rate catalytic windward centerline temperature profiles. The catalycity of TABI is higher than that of ACC, and this causes a temperature spike at the ACC–TABI interface. The surface temperature along the TABI is nearly as high as the fully catalytic profile. The finite rate catalytic temperature spike at the ACC–TABI interface actually exceeds the fully catalytic temperature but is still slightly below the maximum reuse temperature limit.

In-Depth Conduction and TPS Sizing

Finite rate catalytic, radiative equilibrium heat flux and surface temperature at each of the five trajectory points were provided as input to OMLITS. The 92.6-km-altitude trajectory point was selected as the starting point for the time integration. The heat fluxes were assumed to be zero at this point. The heat soak was allowed to continue 2000 s after this initial point. The vehicle is assumed to be on the ground with no incoming heat flux at this time.

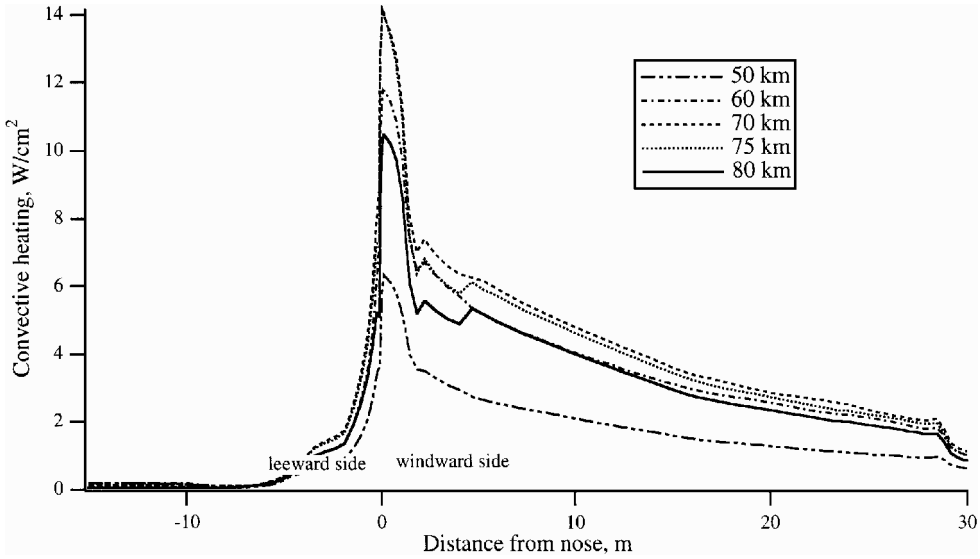

Fig. 8 Finite rate catalytic, radiative equilibrium wall centerline heating profiles.

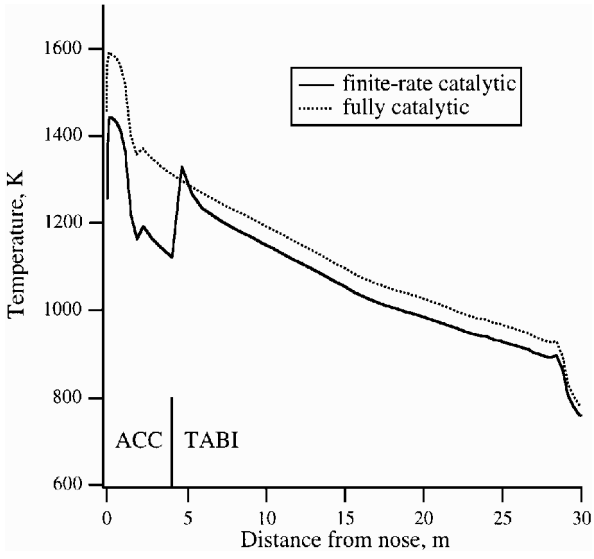

Fig. 9 Windward centerline temperature profiles, 75-km altitude.

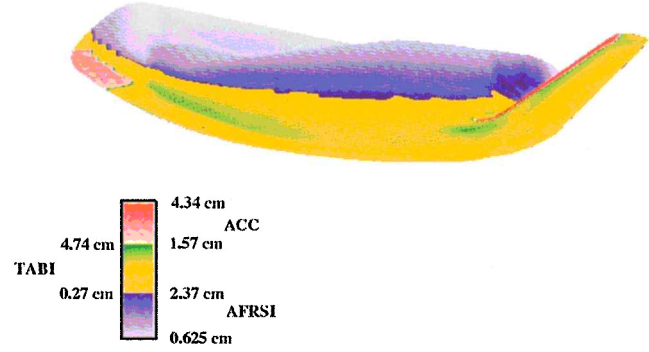

Fig. 10 TPS material thicknesses.

The other input to OMLITS consists of the material stackup at each surface point. The stackup consists of the structural material and either one or two TPS materials. The structural concept for the SSTO lifting-body configuration was modeled as skin–stringer–frame-stiffened construction with an integral tank design. Both the LOX and the hydrogen tank were Al–Li alloy, with the forward compartment, intertank, and thrust structure assumed to be graphite–epoxy. Local-equivalent heat-sink thicknesses, or t-bars, were computed at each body point on the basis of anticipated bending, hoop stress, and longitudinal loading.

The solution process begins with an initial estimate of the outer-layer (ACC, TABI, or AFRSI) TPS thickness at each body point. The time integration then is performed over the entire trajectory. The temperature at the bottom of the material layer, or backface temperature, is computed for each layer in the material stackup. On the basis of these temperatures, the outer-layer thickness is adjusted and the solution recomputed until the limiting bond or material temperature is within 10 K, on the low side, of its maximum value. The maximum bond temperatures for graphite–epoxy and Al–Li are 450 and 395 K, respectively. The material temperature limit for Rhoacell foam is 478 K.

The resulting TPS material thicknesses are shown in Fig. 10. The AFRSI thicknesses are shown in blue. The largest thicknesses of AFRSI occur along the TABI–AFRSI junction and near the wing root, where the thickness is 23.8 mm. The TABI thicknesses are shown in colors ranging from yellow to green. The maximum TABI thickness is 47.4 mm and occurs at the wing root. The ACC thicknesses are shown in red. The thickest layer of ACC, 43.4 mm, is found on the wing leading edge. The maximum thickness in the nose region is 28.0 mm.

Figure 11 shows TPS material thickness profiles along the windward centerline and circumferentially at a distance of 1.7 m from the nose. Along the windward centerline, there is a sharp jump in TPS thickness at the ACC–TABI interface. There is another jump in TPS thickness in the LOX tank region. Here, the TPS is sized by the material limit of the Rhoacell foam and because the Rhoacell foam acts as an insulator to the structure. There are spikes in the circumferential-plane TPS thickness at the ACC–TABI interface probably because of differences in material catalycity.

The OMLITS code also can provide temperature profiles through the material stackup. The time evolution of the temperature profile at windward-side body locations near the stagnation point and at the bottom of the LOX tank is shown in Fig. 12. Figure 12a shows the temperature history for an ACC/graphite–epoxy stackup near the stagnation point. The outer surface temperature increases until the 75-km point and then decreases as the vehicle descends further. The profile is relatively flat 2000 s after the 92.6-km trajectory point when the vehicle is assumed to be on the ground. Because of heat soak, the bondline temperature increases until the 50-km trajectory point. The bondline temperature at the ground point is only slightly lower than this value.

Figure 12b shows the temperature-profile history at a body point located at the bottom of the LOX tank. This is a three-layer material stackup consisting of TABI, Rhoacell foam, and Al–Li. The parameter that drives the TPS sizing here is the material temperature limit of the Rhoacell foam. The surface temperature peaks at 75 km. Because of heat soak, the maximum foam temperature is not reached until 50 km.

An important part of the TPS sizing methodology is to evaluate the grid dependence of the gasdynamic solutions. Finite rate catalytic

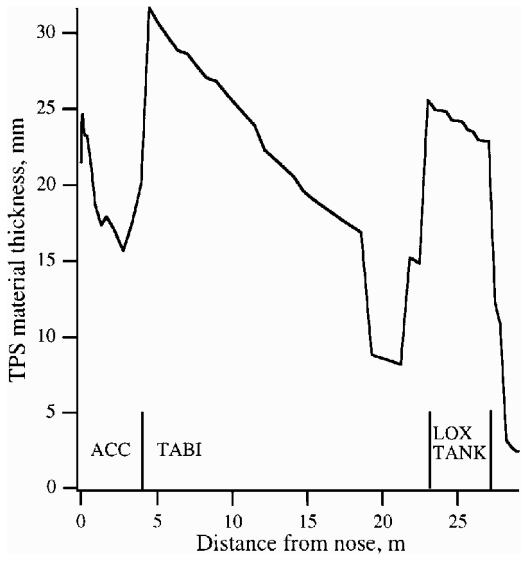

a) Windward centerline

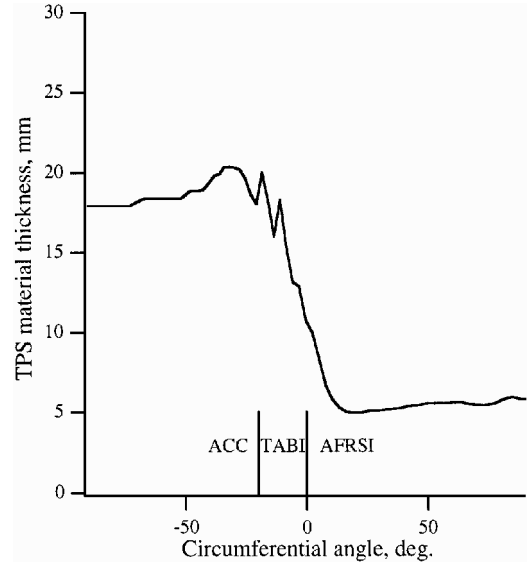

b) Circumferential plane, $x = 1.7$ m from nose

Fig. 11 TPS thickness profiles.

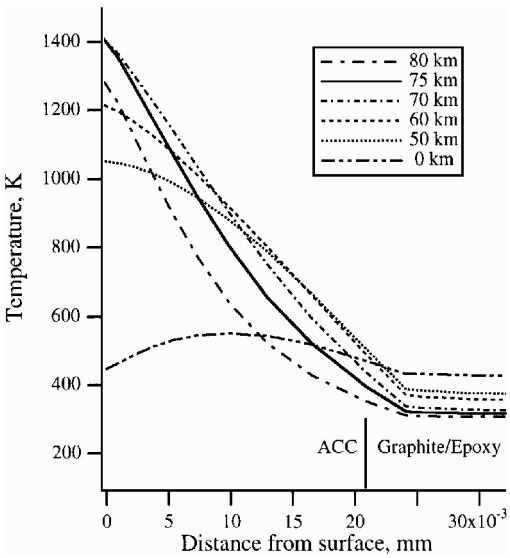

a) Near-stagnation point

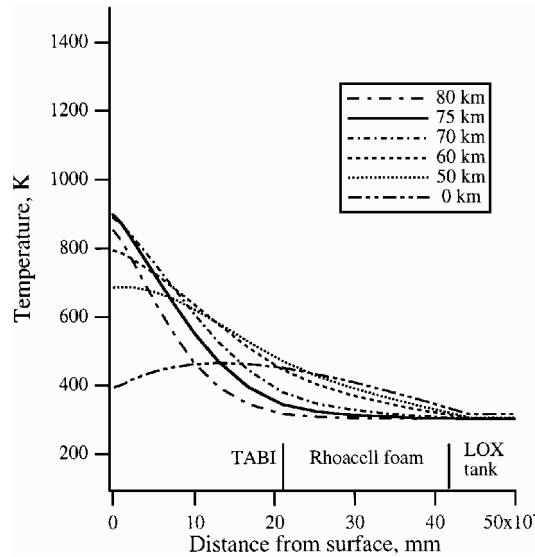

b) Bottom of LOX tank

Fig. 12 In-depth temperature profiles.

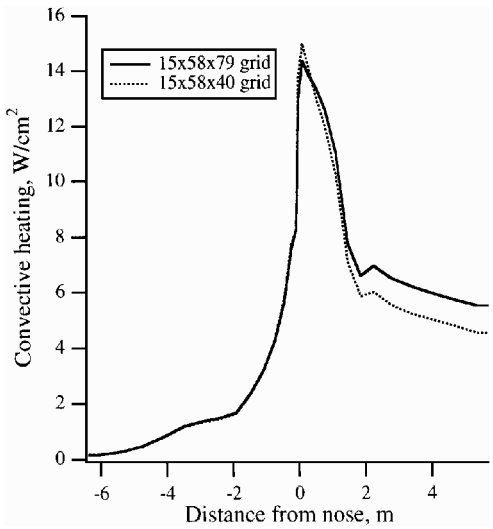

a) Heating, windward centerline

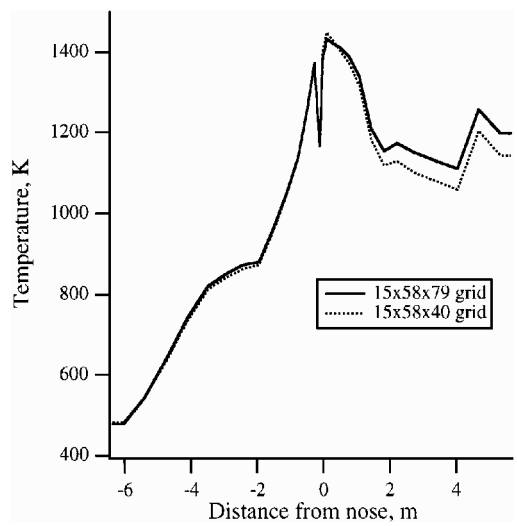

b) Temperature, windward centerline

Fig. 13 Grid resolution study, nose region.

Table 1 TPS material acreage and mass

Material	Surface area, m^2	Mass, kg
ACC	24.5	963.3
TABI	534.0	2137.4
AFRSI	625.8	759.0
Rhoacell	629.9	802.0
Total	1184.3	4661.7

computations were performed using two three-dimensional volume grids. The first was a $15 \times 58 \times 79$ grid created using the first 15 axial lines of the grid used for all previous flow computations in this study. The second grid used the same point-distribution function with half the number of grid points in the body-normal direction. Surface heating and temperature are most sensitive to resolution in the body-normal direction.

Figure 13 shows heating and temperature profiles at the 70-km trajectory point. The coarse grid predicts a stronger windward-side expansion than the fine grid, but the stagnation-region and leeward-side profiles are nearly identical. This study only considered the nose region of the vehicle and does not represent a comprehensive grid-dependence evaluation. A more complete study would entail looking at different locations of the body using additional grid densities, but because the main focus of this paper is to present the high-fidelity TPS sizing methodology, this was not done.

Using the TPS thicknesses and material densities, it is possible to estimate the overall mass of the TPS. The densities of ACC, TABI, and AFRSI are 1660, 160, and 149 kg/m^3, respectively. The minimum gauge thicknesses for TABI and AFRSI are 12.7 and 6.35 mm, respectively. Where the computed TPS thicknesses were below these values, primarily on the leeward surface, the minimum gauge thickness was used instead. Table 1 lists surface area and mass for each material. The overall TPS mass of 4661.7 kg yields a TPS mass per unit area of 3.94 kg/m^2. Note that the overall TPS mass figure only accounts for the primary TPS component of the material stackup and does not take into account such things as strain-isolation-pad or bonding-material mass.

Summary and Conclusions

A methodology is presented to perform a high-fidelity aerothermal and TPS sizing analysis. The procedure is applied to a lifting-body, SSTO vehicle. The gasdynamic flow solver GASP was used to define the flow environment around the vehicle at five points along its descent trajectory. On the basis of computed surface temperatures, TPS materials were mapped on the vehicle surface. The one-dimensional, in-depth conduction code OMLITS was used to generate transient temperature profiles through the TPS/structure material stackup and to size the outer TPS layer based on bondline or material-temperature-limit criteria. This solution methodology allows for a high-fidelity estimate of TPS mass that will critically impact the design and performance of SSTO vehicles.

References

[1]"Access to Space," Advanced Technology Team, Final Rept., Vols. 1–4, NASA, July 1993.

[2]Urie, D. M., and Elvin, J. D., "Innovative Economic Development and Technology Integration for Single Stage to Orbit (SSTO) Concepts," AIAA Paper 95-0279, Jan. 1995.

[3]Williams, S. D., Curry, D. M., Chao, D., and Pham, V. T., "Analysis of the Shuttle Orbiter Reinforced Carbon–Carbon Oxidation Protection System," NASA TM-104792, 1994.

[4]Calamito, D. P., "Development of Tailorable Advanced Blanket Insulation for Advanced Space Transportation Systems," NASA CR-177444, 1987.

[5]Sawko, P. M., and Goldstein, H. E., "Performance of Uncoated AFRSI Blankets During Multiple Space Shuttle Flights," NASA TM-103892, 1992.

[6]Steinbrenner, J. P., and Chawner, J. R., "The GRIDGEN Version 9 Multiple Block Grid Generation Software," MDA, Engineering Rept. 94-01, June 1994.

[7]Walters, R. W., Slack, D. C., Cinnella, P., Applebaum, M., and Frost, C., "A User's Guide to GASP," Virginia Polytechnic Inst. and State Univ., Research Rept. on NASA Grants NAG-1-766 and NAG-1-1045, Blacksburg, VA, Nov. 1990.

[8]Svehla, R. A., and McBride, B. J., "FORTRAN IV Computer Program for Calculation of Thermodynamic and Transport Properties of Complex Chemical Systems," NASA TN-D-7056, 1973.

[9]Blottner, F. G., Johnson, M., and Ellis, M., "Chemically Reacting Viscous Flow Program for Multi-Component Gas Mixtures," Sandia National Lab., SC-RR-70-754, Albuquerque, NM, June 1971.

[10]Anderson, W. K., Thomas, J. L., and Van Leer, B., "Comparison of Finite Volume Flux Vector Splittings for the Euler Equations," *AIAA Journal*, Vol. 24, No. 9, 1986, pp. 1453–1460.

[11]Yee, H. C., Klopfer, G. H., and Montagne, J.-L., "High-Resolution Shock-Capturing Schemes for Inviscid and Viscous Hypersonic Flows," *Journal of Computational Physics*, Vol. 88, No. 1, 1990, pp. 31–61.

[12]Olynick, D., and Henline, W., "Numerical Benchmarks for Navier–Stokes Heating Calculations on Access-to-Space Vehicles," AIAA Paper 95-2078, June 1995.

[13]Henline, W., Palmer, G., and Olynick, D., "Aerothermodynamic Heating Analysis and Heatshield Design of an SSTO Rocket Vehicle for Access-to-Space," AIAA Paper 95-2079, June 1995.

[14]Stewart, D. A., Rakich, J. V., and Chen, Y. K., "Flight Experiment Demonstrating the Effect of Surface Catalysis on the Heating Distribution over the Space Shuttle Heat Shield," *Orbiter Experiments (OEX) Aerothermodynamics Symposium*, edited by D. A. Throckmorton, NASA CP-3248, Pt. 2, 1993, pp. 677–702.

[15]Milos, F. S., Henline, W. D., and Chen, Y.-K., "Numerical Methodology for Full-Body TPS Sizing for Access-to-Space Vehicles," AIAA Paper 96-0614, Jan. 1996.

[16]Gnoffo, P., Weilmuenster, K., and Alter, S., "Multiblock Analysis for Shuttle Orbiter Re-Entry Heating from Mach 24 to Mach 12," *Journal of Spacecraft and Rockets*, Vol. 31, No. 3, 1994, pp. 367–377.

[17]Olynick, D. R., and Tam, T., "Trajectory Based Validation of the Shuttle Heating Environment," AIAA Paper 96-1891, June 1996.

[18]Stewart, D. A., Rakich, J. V., and Lanfranco, M. J., "Catalytic Surface Effects on Space Shuttle Thermal Protection System During Earth Entry of Flights STS-2 Through STS-5," NASA CP-2283, 1983.

B. A. Bhutta
Associate Editor

Color reproduction courtesy of NASA Ames Research Center